symmetry

MDPI

Article

Inductance Analysis of Two-Phase Winding Segmented Permanent Magnet Linear Synchronous Motor

Tuanshan Zhang [1,2] and Xuesong Mei [1,*]

[1] Department of Mechanical Engineering, Xi'an Jiaotong University, Xi'an 710049, China; zhangtuanshan@xpu.edu.cn or zhangtuanshan@stu.xjtu.edu.cn
[2] Department of Mechanical and Electrical Engineering, Xi'an Polytechnic University, Xi'an 710048, China
* Correspondence: xsmei@mail.xjtu.edu.cn

Abstract: The inductance of a winding segmented permanent magnet linear synchronous motor (WS-PMLSM) is affected by winding disconnection and coupling length variation, which makes the variation of inductance more complicated, and this paper proposes incremental inductance, apparent inductance, and positional inductance to reveal this phenomenon, which gives a theoretical basis for mathematical modeling and thrust fluctuation suppression. First, an analytical approach is used to derive a fully coupled state model using the magnetomotive force and specific permeability function. Second, the domain of the specific permeability function is extended and the inductance expressions are calculated for the whole moving range. Finally, the inductance of the prototype WS-PMLSM with a two-phase winding is experimentally verified, and it is proposed that the effects of the three inductive components on the system should be considered comprehensively when implementing control of the WS-PMLSM.

Keywords: inductance; winding segmented permanent magnet linear synchronous motor; magnetomotive force; specific permeability function

Citation: Zhang, T.; Mei, X. Inductance Analysis of Two-Phase Winding Segmented Permanent Magnet Linear Synchronous Motor. *Symmetry* **2022**, *14*, 1180. https://doi.org/10.3390/sym14061180

Academic Editor: Jan Awrejcewicz

Received: 8 May 2022
Accepted: 2 June 2022
Published: 8 June 2022

1. Introduction

A WS-PMLSM is a motor with special characteristics and imagination, which is one of the innovative works of the linear motor by connecting the stator of the motor in series and making the movable element run independently. Due to its unique advantages, it was first used in modern industrial material transfer lines and in generating assembly lines, represented by the Rexroth active mover transfer system [1]. Figure 1 shows a simple example of a combination of transporting and processing material with linear transport, the linear transport system must have the following characteristics: the track must allow for horizontal and vertical curves, thus forming a closed path; process handling stations (P1 . . . P3) are distributed along the track; on the carriageway, the multiple movers (workpiece transporters, V1 . . . V4) must be able to travel simultaneously and with a high degree of independence.

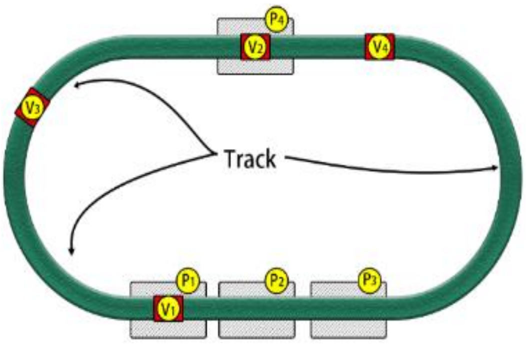

Figure 1. Simple example of the proposed linear drive system.

While the WS-PMLSM can provide some benefits, it does present challenges in implementing smooth control and motor modeling, especially when the mover covers multiple stators simultaneously [2], the electromagnetic relations lead to the failure of classical motor models, thus exacerbating thrust fluctuations [3–7]. The motor with a WS-PMLSM structure has the following characteristics:

1. The WS-PMLSM has an offset pulsating magnetic field [8] due to the adjacent segment cores, which will cause the magnetic field at the yoke near the energized segment to saturate easily and the inductance of the motor will be unbalanced, which will make the inductance and position in the $dq0$-based algorithm not decoupled and a sinusoidal function will appear in the equation [9].
2. During motor operation, when the mover overlaps with parts of two or three stator segments, the inductance variation of the stator contains multiple harmonics, this will produce a position-dependent inverse electric potential (EMF) constant [10].

In the field of WS-PMLSM-related technology, some scholars have done a lot of work, including the integrated application of space vector, direct torque, tooth slot resonance, and segmental feedforward methods, as well as the control of accurate feedforward combined with finite element model, absolute position acquisition, etc., which are summarized as follows:

1. The current in the transition section must have the same amplitude and phase [11].
2. The current of the transition section should adopt the "master-slave" follow mode [12].
3. Transitional inductance should be solved by a look-up table method [13].
4. Thrust fluctuation adopts feedforward or online identification iteration, disturbance observer [3].
5. Optimal control with consistent energy consumption and thrusts [14].

Due to the presence of uncoupled semi-open domain magnetic fields in the primary WS-PMLSM and smooth cross-sectional crossings between the primary segments, these special phenomena make the characteristics of inductance in the WS-PMLSM different from the conventional primary continuous PMLSM. Therefore, it is very important to study the inductance variation law in its motion range and obtain an accurate inductance model, which is the only way to ensure high-speed motion and high-precision positioning, such as the XTS transmission system developed by Beckhoff [15] with a maximum speed of 4 m/s and repetitive positioning accuracy of less than 10 um.

The calculation methods of inductance mainly include direct method [16,17] and indirect method [18,19]. The direct method firstly solves the Poisson equation of the magnetic field to obtain the vector magnetic potential, and then calculates the analytical expression of the inductance through the magnetic field energy storage. However, for the WS-PMLSM, this method has difficulties in determining boundary conditions and complex equations [20]; the indirect method is a method of calculating inductance by integrating the product of the winding function (magnetic potential function) and the air gap ratio permeability function. Compared with the direct method, the indirect method is simpler and more intuitive when calculating the motor inductance, but its solution accuracy depends on the accuracy of the air gap ratio permeability function [21]. Many studies [22,23] have investigated the inductance of rotating motor using indirect methods. For WS-PMLSM, some studies [11,24,25] have studied the transition inductance of WS-PMLSM with three-phase structure. Due to the effects of winding discontinuity and coupling length variation, these studies only describe the effect of complex transition inductance on thrust and do not indicate the actual operability, while very few studies have been conducted on the transition inductance of two-phase WS-PMLSM. In this paper, an indirect method is used to calculate the inductance of the motor while considering these influencing factors.

In this paper, based on the classical MMF theory, the MMF distribution of the single-phase winding of the segmented linear motor is derived, the MMF distribution characteristics of the segmented linear motor are elucidated, and derive the manufacturing requirements and formula derivation for segmented linear motors with sinusoidal windings. Based on the magnetic field distribution of the motor, the expressions for the self and mutual inductance of each phase winding of the motor are derived to explain the mutual inductance asymmetry mechanism of the segmented linear motor. The motor inductance matrix obtained on this basis solves the special characteristics of mutual inductance and impedance of the WS-PMLSM. The proposed inductance matrix is also experimentally verified.

2. Motor Model

Two-phase motors are used more in stepper motors and have not yet attracted attention in the field of linear motors. From a structural point of view, two-phase has more advantages than three-phase, as summarized below:

1. The two-phase motor is phase-balanced because the magnetic circuit is the same in each phase. Therefore, it eliminates the phase asymmetry problem caused by half-filled slots, which is common in three-phase linear motors.
2. Although motors with two-phase windings are not advantageous in the design of rotary motors, the advantages of two-phase windings are obvious in linear motors, the span of the winding is smaller than that of the three-phase, the two windings are spatially perpendicular to each other, there are no Clark and anti-Clark transformations, the speed of vector control implementation is accelerated, and the general embedded system can meet the requirements.
3. The two-phase winding can be easily made into a single layer winding, and since only one winding is embedded in each stator slot along the active side of the coil, the inductance is basically physically balanced, which also makes the process simple, the full slot rate high, and the windings can be made in concentric mode to achieve the physical structure of a sinusoidal winding and reduce harmonics.

The two-phase motor designed in this paper is shown in Figure 2 below. A stator module consists of five two-phase segmented windings [2], each segmented winding is equivalent to a two-phase motor, phases coil winding are wound at equal intervals on the stator tooth slot with a spatial electrical angle of 90, and a mover consisting of a permanent magnet and an iron core, the size of which covers a complete one segmented stator.

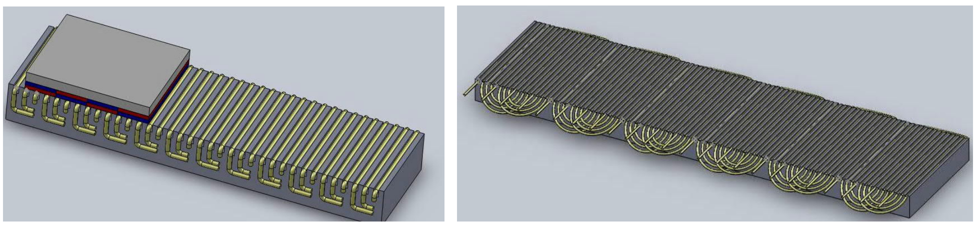

(**a**) (**b**)

Figure 2. Motor model. (**a**) Physical drawing of winding structure; (**b**) schematic of the WS-PMLSM.

The stator of a two-phase long armature linear motor is composed of multiple segments, the number of segments from left to right is $1 \sim N_{sec}$. The parameters of the WS-PMLSM are given in Table 1.

Before deriving the formula, first, define two coordinate systems, one is the stator coordinate system $\alpha - \theta_s$ and the other is the mover coordinate system $\beta - \theta_r$, and the distance between the two coordinate systems is θ. The schematic diagram of the two coordinate systems of WS-PMSLM is shown in the Figure 3, the $\alpha - \theta_s$ coordinate system is fixed on the stator with the α-axis coinciding with the center of the A-phase winding, and the $\beta - \theta_r$ coordinate system is fixed on the mover with the β-axis coinciding with the center of the permanent magnet. All the angles are defined as electrical angles, and the conversion relationship between the angles of the two coordinate systems is $\theta_s = \theta_r + \theta$.

Table 1. Parameters of the WS-PMLSM.

Description	Symbol	Value	Unit
Length of segmented stator	$2\ \tau$	100	mm
Pitch of permanent magnet	τ	50	mm
Pitch of coil	τ_c	50	mm
Turn of coil	n	10	$turns/slot$
Resistance of coil	R	2.55	ohm/phase
Inductance of coil	L	16.9	mH/phase
Number of poles	$number$	2.3	any combination
Connection pattern	$node$	star/tri	any combination
Stator materials			35JN470
Magnet materials			35SH
Magnet residual magnetic	B_r/T	1.15	T
Magnet coercive force	H_{cj}	1672	$\mathrm{KA/m^{-1}}$
Mover yoke materials			35JN470

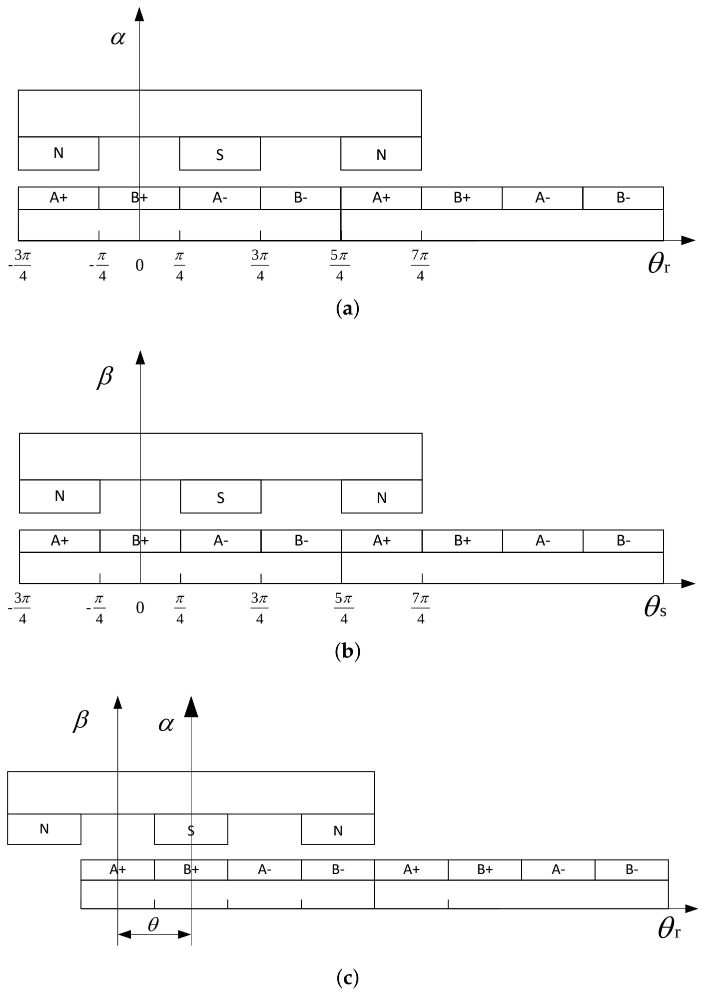

Figure 3. Two coordinate systems and their relationships. (**a**) Stator coordinate system; (**b**) mover coordinate system; (**c**) coordinate distance.

3. Inductance and WS-PMLSM Control

The electrical performance of a motor is usually described by a differential equation consisting of the winding voltage, current, and magnetic linkage. The voltage equation of the winding has the following form:

$$u = Ri + \frac{d\lambda}{dt} \tag{1}$$

The magnetic linkage λ is not only related to the current of the winding but is also a function of the mover position angle (linear motors are displacement) θ_r, thus Equation (1) can be written as:

$$u = Ri + \frac{\partial\lambda}{\partial i} \cdot \frac{di}{dt} + \frac{\partial\lambda}{\partial\theta_r} \cdot \frac{d\theta_r}{dt} = Ri + L^{inc} \cdot \frac{di}{dt} + \frac{\partial L^{opp}}{\partial\theta_r} \cdot \frac{d\theta_r}{dt} \tag{2}$$

where

$$L^{inc} = \frac{\partial\lambda}{\partial i}, \quad L^{opp} = \frac{\lambda}{i} \tag{3}$$

L^{opp} is the apparent inductance, which is commonly referred to as inductance, and L^{inc} can be called incremental inductance. They are equal only if the magnetic circuit is unsaturated and in the linear region. Therefore, at full range, using L instead of L^{opp} and L^{inc} necessarily introduces errors to the performance analysis of the motor. In addition, the existing formulae for calculating motor parameters are only applicable to the conventional case of sinusoidal distribution of the air-gap magnetic field and do not consider the stator and rotor tooth slots, as well as the asymmetry of the air-gap or windings.

With the application of computers, power electronics, and automatic control technology in the electromechanical industry, the structure type and operation mode of the motor are changing, the voltage and current of the power supply are often no longer sinusoidal, and it is necessary to change the consideration of winding potential harmonics and air gap conductivity harmonics in the steady-state and transient analysis of motor. The traditional method of calculating motor inductance can no longer meet the requirements, and a more accurate and general method of calculating motor inductance must be found. The authors of [22] propose a magnetic energy perturbation method but only consider the incremental inductance.

Since the WS-PMLSM with two-phase stator structure is used for the study, the equations of the magnetic circuit in the stationary two-phase stator $\alpha-\beta$ coordinate system are as follows:

$$\vec{u}_{\alpha\beta} = \mathbf{R}_{\alpha\beta} \cdot \vec{i}_{\alpha\beta} + \frac{d\vec{\Psi}_{\alpha\beta}}{dt} \tag{4}$$

$$\vec{u}_{dq} = \begin{bmatrix} u_d \\ u_q \end{bmatrix} = \underbrace{\begin{bmatrix} \cos(\theta) & \sin(\theta) \\ -\sin(\theta) & \cos(\theta) \end{bmatrix}}_{\mathbf{T_{dq}}} \cdot \vec{u}_{\alpha\beta} \tag{5}$$

$$\vec{u}_{\alpha\beta} = \underbrace{\begin{bmatrix} \cos(\theta) & -\sin(\theta) \\ \sin(\theta) & \cos(\theta) \end{bmatrix}}_{\mathbf{T_{dq}^{-1}}} \cdot \vec{u}_{dq} \tag{6}$$

with $\theta = \frac{\pi}{\tau_p} \cdot x$, and τ_p the pole pitch of the linear motor. Returning to the $\alpha-\beta$ coordinate system, the flux linkage depends on the current and the position x:

$$\vec{\Psi}_{\alpha\beta} = \mathbf{L}_{\alpha\beta}\left(\vec{i}_{\alpha\beta}, x\right) \cdot \vec{i}_{\alpha\beta} + \vec{\Psi}_{\alpha\beta PM}(x) = \begin{bmatrix} L_{\alpha\alpha} & L_{\alpha\beta} \\ L_{\beta\alpha} & L_{\beta\beta} \end{bmatrix} \cdot \begin{bmatrix} i_\alpha \\ i_\beta \end{bmatrix} + \begin{bmatrix} \Psi_{\alpha PM} \\ \Psi_{\beta PM} \end{bmatrix} \tag{7}$$

In Equation (7), the inductance matrix depends on the saturation of the core and is a function of current and position. The flux linkage represents the magnetic flux produced by the magnet. Applying the transformation of Equation (7) in Equation (6) yields Equation (8):

$$\vec{\Psi}_{dq} = \underbrace{\mathbf{T}_{\alpha\beta-\mathbf{dq}} \cdot \mathbf{L}_{\alpha\beta} \cdot \mathbf{T}^{-\mathbf{s}}_{\alpha\beta-\mathbf{dq}}}_{\mathbf{L_{dq}}} \cdot \vec{i}_{dq} + \vec{\Psi}_{dqPM}(x) \tag{8}$$

$$\vec{u}_{dq} = \underbrace{\mathbf{T_{dq}} \cdot \mathbf{R}_{\alpha\beta} \cdot \mathbf{T_{dq}^{-1}}}_{\mathbf{R_{dq}}} \cdot \vec{i}_{dq} + \mathbf{T_{dq}} \cdot \frac{d\left(\mathbf{T_{dq}^{-1}} \cdot \vec{\Psi}_{dq}\right)}{dt} \tag{9}$$

$$\vec{u}_{dq} = \mathbf{R}_{\mathrm{dq}} \cdot \vec{i}_{dq} + \frac{d\vec{\Psi}_{dq}}{dt} + \frac{\pi}{\tau_p} \cdot \begin{bmatrix} 0 & -1 \\ 1 & 0 \end{bmatrix} \cdot \vec{\Psi}_{dq} \cdot \frac{dx}{dt} \tag{10}$$

Its matrix components are as follows:

$$\begin{array}{l} \Psi_d = L_{dd} \cdot i_d + L_{dq} \cdot i_q + \Psi_{dPM} \\ \Psi_q = L_{qd} \cdot i_d + L_{qq} \cdot i_q + \Psi_{qPM} \\ \frac{\partial \Psi_d}{\partial i_d} = \frac{\partial L_{dd}}{\partial i_d} \cdot i_d + L_{dd} + \frac{\partial L_{dq}}{\partial i_d} \cdot i_q \\ \frac{\partial \Psi_d}{\partial i_q} = \frac{\partial L_{dd}}{\partial i_q} \cdot i_d + L_{dq} + \frac{\partial L_{dq}}{\partial i_q} \cdot i_q \\ \frac{\partial \Psi_q}{\partial i_q} = \frac{\partial L_{qd}}{\partial i_d} \cdot i_d + L_{qd} + \frac{\partial L_{qq}}{\partial i_d} \cdot i_q \\ \frac{\partial \Psi_q}{\partial i_q} = \frac{\partial L_{qd}}{\partial i_q} \cdot i_d + L_{qq} + \frac{\partial L_{qq}}{\partial i_q} \cdot i_q \end{array} \tag{11}$$

The linked flux vector $\vec{\Psi}_{dq}$ is a function of $\vec{i}_{dq}$ and x. Then, the derivative can be rewritten as in Equation (12).

$$\frac{d\vec{\Psi}_{dq}}{dt} = \frac{\partial \vec{\Psi}_{dq}}{\partial \vec{i}_{dq}} \cdot \frac{d\vec{i}_{dq}}{dt} + \frac{\partial \vec{\Psi}_{dq}}{\partial x} \cdot \frac{dx}{dt} \tag{12}$$

$$\frac{\partial \vec{\Psi}_{dq}}{\partial \vec{i}_{dq}} = \begin{bmatrix} \frac{\partial L_{dd}}{\partial i_d} \cdot i_d & \frac{\partial L_{dd}}{\partial i_q} \cdot i_d \\ \frac{\partial L_{qd}}{\partial i_d} \cdot i_d & \frac{\partial L_{qd}}{\partial i_q} \cdot i_d \end{bmatrix} + \begin{bmatrix} \frac{\partial L_{dq}}{\partial i_d} \cdot i_q & \frac{\partial L_{dq}}{\partial i_q} \cdot i_q \\ \frac{\partial L_{qq}}{\partial i_d} \cdot i_q & \frac{\partial L_{qq}}{\partial i_q} \cdot i_q \end{bmatrix} + \begin{bmatrix} L_{dd} & L_{dq} \\ L_{qd} & L_{qq} \end{bmatrix} = \mathbf{L}_{\mathrm{dq}}^{\mathrm{diff}} \tag{13}$$

From Equation (12), it can be seen that the inductance matrix $\mathbf{L}_{\mathrm{dq}}^{\mathrm{diff}}$ consists of apparent inductance and incremental inductance.

$$\frac{\partial \vec{\Psi}_{dq}}{\partial x} = \frac{\partial \mathbf{L_{dq}}}{\partial x} \cdot \vec{i}_{dq} + \frac{\partial \vec{\Psi}_{dqPM}}{\partial x} \tag{14}$$

As seen in Equation (14), the variation of the inductance matrix with position is also a term in Equation (14). Introducing Equations (12)–(14) into Equation (10), the voltage equation of the motor is rewritten as in Equation (15).

$$\vec{u}_{dq} = \mathbf{R}_{\mathrm{dq}} \cdot \vec{i}_{dq} + \mathbf{L}_{\mathrm{dq}}^{\mathrm{diff}} \cdot \frac{d\vec{i}_{dq}}{dt} + \underbrace{\left(\frac{\partial \vec{\Psi}_{dq}}{\partial x} + \frac{\pi}{\tau_p} \cdot \begin{bmatrix} -\Psi_q \\ \Psi_d \end{bmatrix} \right) \cdot \frac{dx}{dt}}_{EMF} \tag{15}$$

From Equation (15), the different types of voltage drops can be identified: resistive voltage drop $R_{dq} \cdot \vec{i}_{dq}$, inductive voltage drop $\mathbf{L}_{\mathrm{dq}}^{\mathrm{diff}} \cdot \frac{d\vec{i}_{dq}}{dt}$ and back EMF. In summary, there are several characteristics of inductance in motor control as follows:

1. The inductance becomes an inductance matrix-$\mathbf{L}_{\mathrm{dq}}^{\mathrm{diff}}$, also known as the differential inductance array, which consists of apparent inductance and incremental inductance.
2. The apparent inductance-$\mathbf{L_{dq}}$, is a constant in conventional motor, but in the WS-PMLSM, it is a function of position and current.
3. In Equation (13), the differential inductance minus the apparent inductance is the incremental inductance, which can be ignored in the linear motor
4. $\frac{\partial \mathbf{L_{dq}}}{\partial x}$ indicates the variation of inductance with position, which can generally be obtained by curve fitting.

It can be seen that in the mathematical model of the motor, the inductance matrix has three variables: apparent inductance, incremental inductance, and position inductance.

4. Apparent Inductance of Motor

According to the above analysis, the apparent inductance is independent of the current and can be analyzed by the magnetic circuit method. In this way, a hierarchical model can be used to derive the air gap permeability, magnet, and motor winding potentials to calculate the inductance in the initial design and performance evaluation of the motor.

4.1. Motor Winding

The motor proposed in this paper is still a relatively new structure, and the special winding structure of the motor can also partially solve the inductive nonlinear characteristics, so its winding structure is introduced first.

The following focuses on the method of generating a sinusoidal magnetic potential for two-phase windings. The core of this method is the use of concentrically arranged distributed windings so that an MMF with sinusoidal distribution can be obtained by using differently spaced windings in one pole pitch. such concentric windings and their MMF is shown in Figure 4. Since the phase relationship between the MMF is the same as the spatial relationship of the coils, the phase of the MMF is the sum of the MMF of each coil. Although the MMF obtained is stepped, the MMF approximates a sinusoidal wave due to the filtering effect of the inductor. The advantage of concentric winding is that it is easy to produce and maintain, and produces an approximately sinusoidal moving MMF distribution, but its disadvantage is that the effective number of turns of the winding is less than the sum of the coil turns.

Figure 4 shows the unfolding diagram of phase A winding with coils uniformly distributed, the total number of turns of this phase is set to T_{ph}, then the number of coils at any position θ in space is.

$$N_s = \begin{cases} (-1)^k N_0 & -\frac{3\pi}{4} + k\pi < \theta < -\frac{\pi}{4} + k\pi \\ 0 & -\frac{\pi}{4} + k\pi < \theta < \frac{\pi}{4} + k\pi \\ & k = 0, 1, 2 \cdots n \end{cases} \tag{16}$$

In the formula, $N_0 = \frac{T_{ph}}{16}$, so the number of coil per pole is:

$$N_p = 8N_0 = \frac{T_{ph}}{2} \tag{17}$$

N_s is an odd function in the defined interval, expanded in the form of a Fourier series:

$$N_s(\theta) = \sum_{n=1}^{\infty} b_n \sin(n\theta) \tag{18}$$

The Fourier coefficients are as follows:

$$b_n = \frac{2}{T} \int_{\theta_0}^{\theta_0+T} N_s(\theta) \sin n\theta d\theta = \frac{2N_0}{n\pi} \left(\cos \frac{3\pi n}{4} - \cos \frac{\pi n}{4} \right) \tag{19}$$

where $T = 2\pi$, it can be introduced from the above equation:

$$N_s(\theta) = \sum_{n=1}^{\infty} \frac{2N_0}{n\pi} \left(\cos \frac{3\pi n}{4} - \cos \frac{\pi n}{4} \right) \sin(n\theta) = \sum_{n=1}^{\infty} T_{ph} \sin(n\theta) \; (n = 1, 3, 5, \cdots) \tag{20}$$

In the formula, $T_{ph} = \frac{2N_0}{n\pi} (\cos \frac{3\pi n}{4} - \cos \frac{\pi n}{4})$, then, the MMF generated by coil:

$$F_{\mathrm{as}} = \frac{\sum_{n=1}^{\infty} T_{ph} \sin(n\theta) I_{\mathrm{m}}}{P} \sin(\omega_{\mathrm{s}} t); F_{\mathrm{bs}} = \frac{\sum_{n=1}^{\infty} T_{ph} \sin\left(n\theta - \frac{\pi}{2}\right) I_{\mathrm{m}}}{P} \sin\left(\omega_{\mathrm{s}} t - \frac{\pi}{2}\right) \tag{21}$$

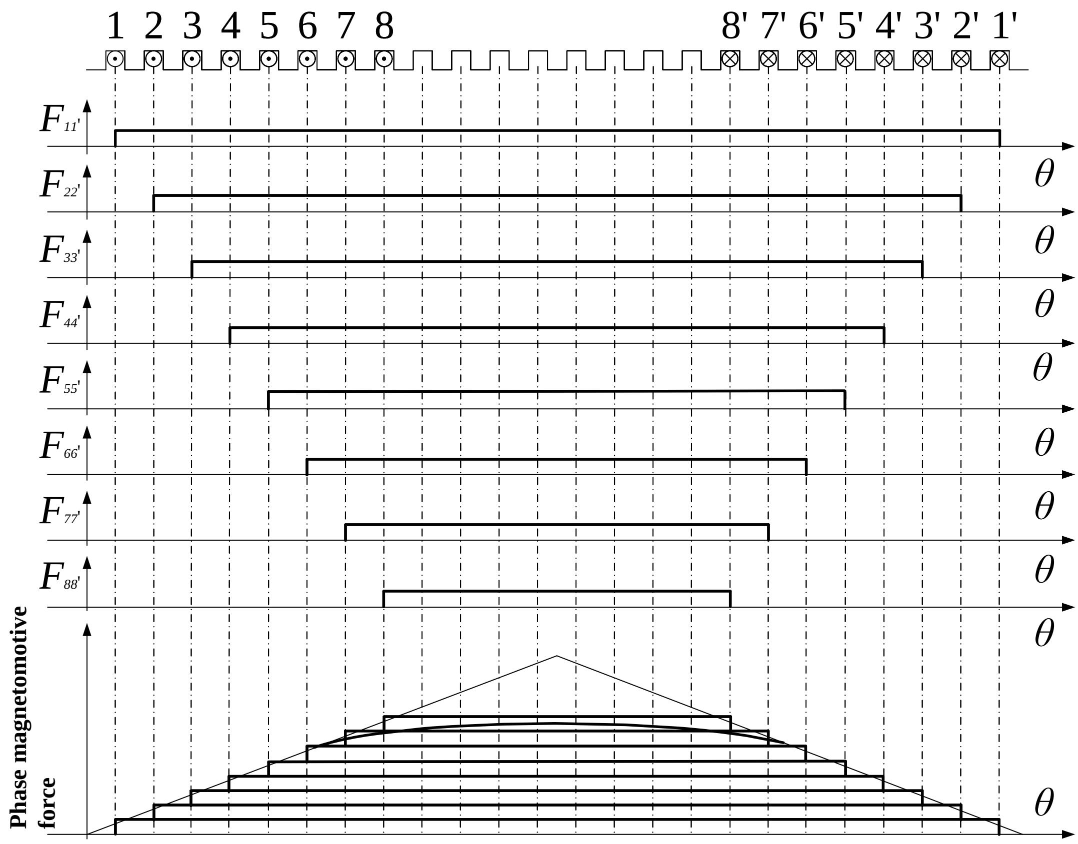

Figure 4. Principle of sinusoidal magnetomotive force.

Since the motor is two-pole, each air gap corresponds to one pole, so that the flux in the magnetic circuit is obtained:

$$F_{\mathrm{as}} = \frac{\sum\limits_{n=1}^{\infty} T_{ph}\sin(n\theta) I_{\mathrm{m}}}{P}\sin(\omega_{\mathrm{s}}t) = \frac{1}{2}\frac{\sum\limits_{n=1}^{\infty} T_{ph} I_{\mathrm{m}}}{P}[\cos(n\theta-\omega_{\mathrm{s}}t)-\cos(n\theta+\omega_{\mathrm{s}}t)] \tag{22}$$

$$F_{\mathrm{bs}} = \frac{\sum\limits_{n=1}^{\infty} T_{ph}\sin\left(n\theta-\frac{\pi}{2}\right) I_{\mathrm{m}}}{P}\sin\left(\omega_{\mathrm{s}}t-\frac{\pi}{2}\right) = \frac{1}{2}\frac{\sum\limits_{n=1}^{\infty} T_{ph} I_{\mathrm{m}}}{P}[\cos(n\theta+\omega_{\mathrm{s}}t)+\cos(n\theta-\omega_{\mathrm{s}}t)] \tag{23}$$

The resultant MMF is:

$$F = F_{\mathrm{as}} + F_{\mathrm{bs}} = \frac{\sum\limits_{n=1}^{\infty} Fphl_{\mathrm{m}}}{P}[\cos(n\theta-\omega_{\mathrm{s}}t)] \tag{24}$$

From Equation (24), it is the sinusoidal traveling MMF.

4.2. Motor Magnets

Figure 5 shows the arrangement order of permanent magnets, i.e., NSN.

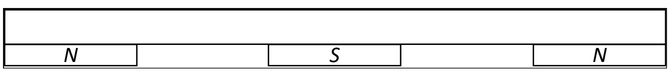

Figure 5. Arrangement of secondary magnets.

From Figure 6, The expansion equation for the potential of permanent magnet is as follows:

$$f(x) = \begin{cases} 0 & k\tau - \frac{\tau-\tau_{\mathrm{p}}}{2} \le x \le k\tau + \frac{\tau-\tau_{\mathrm{p}}}{2} \\ (-1)^{k+1}F_0 & k\tau + \frac{\tau-\tau_{\mathrm{p}}}{2} \le x \le k\tau + \frac{\tau+\tau_{\mathrm{p}}}{2} \\ & k = 0, \pm 1 \end{cases} \tag{25}$$

where τ is the pole distance of the mover; τ_p is the longitudinal length of the permanent magnet. F_0 is the excitation potential of the equivalent coil, and $f(x)$ is an odd function in the defined interval, expanded by Fourier series, where $T = 2\tau$.

$$b_n = \frac{2}{\tau}\int_0^x f(x)\sin\left(\frac{n\pi}{\tau}\right)\mathrm{d}x = \frac{4F_0}{n\pi}(-1)^{\frac{n+1}{2}}\sin\frac{n\pi\alpha}{2} \quad (n = 1, 3, 5, \cdots) \tag{26}$$

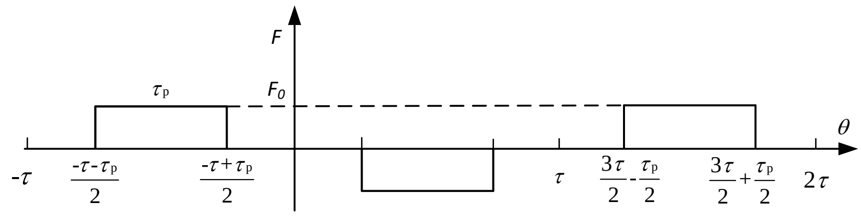

Figure 6. Magnetic potential distribution of PM.

From Figure 6, the function formula of the secondary magnetic potential of the motor is:

$$f(x) = \sum_{n=1}^{\infty}(-1)^{\frac{n+1}{2}}\frac{4F_0}{n\pi}\sin\left(\frac{n}{2}\pi\alpha\right)\sin\left(\frac{n\pi}{\tau}x\right) \tag{27}$$

where: $\alpha = \frac{\tau_p}{\tau}, \theta = \frac{n\pi}{\tau}x$. so $f(\theta)$ can be written:

$$f(\theta) = \sum_{n=1}^{\infty}(-1)^{\frac{n+1}{2}}\frac{4F_0}{n\pi}\sin\left(\frac{n\pi}{4}\right)\sin(n\theta) \tag{28}$$

4.3. Flux Analysis

The special structure of the WS-PMLSM makes it impossible to fully apply the existing formulae for magnetic flux analysis. The magnetic flux of the motor must be analyzed according to the change in the position of the mover. The air-gap flux of the motor is the sum of the flux generated by the excitation of the winding itself and the flux generated by the permanent magnet.

4.3.1. Dynamic Processes

From a practical point of view, there are three cases: the mover is fully coupled to the stator, the mover is partially coupled to the stator, and the mover is completely away from the stator, as shown in Figure 7.

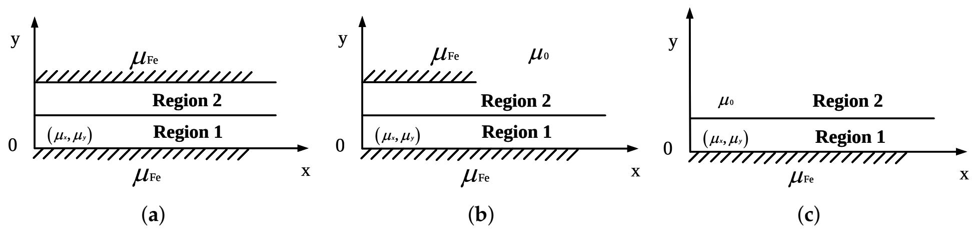

Figure 7. Mover transition process. (**a**) Mover fully couple stator; (**b**) mover partially couple stator; (**c**) mover fully away stator.

4.3.2. Analysis of Air Gap Permeability Coefficient

Since the motor is non-convex, the relative permeabilities of the magnet and air are approximately equal. When calculating the transition inductance, three cases should be considered for the air gap permeability coefficient. One is without mover coupling, which can be set as a constant λ_1, another is mover fully coupled stator, which can be set as a constant λ_2, and the third is mover partial coupling, which can be set as a linear function λ_3.

$$\lambda_1(x) = \frac{\mu_0}{g_h} \tag{29}$$

$$\lambda_2(x) = \lambda_{\text{gap}}(x) + \lambda_{\text{teeth}}(x) \tag{30}$$

The calculation of λ_2 is more complex, Considering the hierarchical model, as shown in Figure 8.

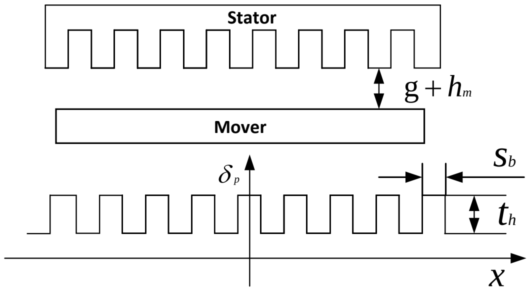

Figure 8. Motor hierarchical model.

The derivation process is as follows:

$$\lambda_{\text{gap}}(x) = \begin{cases} \frac{\mu_0}{g+t_\text{h}} & 0 \le x < \frac{s_\text{b}}{2} \\ \frac{\mu_0}{g} & \frac{s_\text{b}}{2} \le x < \frac{s_\text{b}}{2} + t_\text{b} \\ \frac{\mu_0}{g+t_\text{h}} & \frac{s_\text{b}}{2} + t_\text{b} \le x < s_\text{b} + t_\text{b} \end{cases} \tag{31}$$

$$\lambda_{\text{teeth}}(x) = \begin{cases} 0 & 0 \le x < \frac{s_\text{b}}{2} \\ \frac{\mu_{\text{Fe}}}{t_\text{h}} & \frac{s_\text{b}}{2} \le x < \frac{s_\text{b}}{2} + t_\text{b} \\ 0 & \frac{s_\text{b}}{2} + t_\text{b} \le x < s_\text{b} + t_\text{b} \end{cases} \tag{32}$$

where $\lambda_{\text{gap}}\ (x)$ and $\lambda_{\text{teeth}}\ (x)$ are even functions, $T_2 = s_\text{b} + t_\text{b}$, expanded in the form of Fourier series:

$$\lambda_{\text{gap}}(x) = \frac{\mu_0}{s_\text{b}} + t_\text{b}\left[\frac{s_\text{b}}{g+t_\text{h}} + \frac{t_\text{b}}{g}\right] - \frac{2\mu_0 t_\text{h}}{n\pi g(g+t_\text{h})}\sin\left(\frac{s_\text{b} n\pi}{s_\text{b}+t_\text{b}}\right)\cos\left(\frac{2n\pi x}{s_\text{b}+t_\text{b}}\right)\begin{cases} n = 2k \\ k = 0, 1, 2, \cdots \end{cases} \tag{33}$$

$$\lambda_{\text{teeth}}(x) = \frac{\mu_{\text{Fe}} t_\text{b}}{(s_\text{b}+t_\text{b})t_\text{h}} - \frac{2\mu_{\text{Fe}}}{n\pi t_\text{h}}\sin\left(\frac{n\pi s_\text{b}}{s_\text{b}+t_\text{b}}\right)\cos\left(\frac{2n\pi x}{s_\text{b}+t_\text{b}}\right)\begin{cases} n = 2k, \\ k = 0, 1, 2, \cdots \end{cases} \tag{34}$$

Summing up the above formula, the following formula can be introduced:

$$\begin{aligned} \lambda_2(x) = {} & \frac{\mu_0}{s_\text{b}+t_\text{b}}\left[\frac{s_\text{b}}{g+t_\text{h}} + \frac{t_\text{b}}{g}\right] + \frac{\mu_{\text{Fe}} t_\text{b}}{(s_\text{b}+t_\text{b})t_\text{h}} - \left[\frac{2\mu_0 t_\text{h}}{n\pi g(g+t_\text{h})}\sin\left(\frac{s_\text{b} n\pi}{s_\text{b}+t_\text{b}}\right) + \frac{2\mu_{\text{Fe}}}{n\pi t_\text{h}}\sin\left(\frac{n\pi s_\text{b}}{s_\text{b}+t_\text{b}}\right)\right] \\ & \cos\left(\frac{2n\pi x}{s_\text{b}+t_\text{b}}\right)\begin{cases} n = 2k \\ k = 0, 1, 2, \cdots \end{cases} \end{aligned} \tag{35}$$

During the transition, since the permeability of the permanent magnet is approximately equal to the permeability of air, they can be considered as linear and a straight-line fit is sufficient, as shown below:

$$\lambda_3 = \lambda_1(x) + \frac{\lambda_2(x) - \lambda_1(x)}{\tau_1}x \tag{36}$$

where τ_1 is the length of the stator section of the motor and x is the displacement of the mover with respect to the stator.

4.3.3. Inductance of Motor

We established the Y-axis specific permeability functions λ_1, λ_3 for the fully coupled and uncoupled conditions, and the analytical model of the coupling length variation of the mover transition process λ_2. Then, on the basis of the analytical model, the inductance variation law of the WS-PMLSM in the whole stroke is quantitatively analyzed, and the air-gap density B in the whole process of mover is:

$$B(\theta) = F(\theta)\lambda(\theta) = \begin{cases} F(\theta)\lambda_1 & \theta \le -\frac{3\pi}{4} \\ (F(\theta) + f(\theta))\lambda_3 & -\frac{3\pi}{4} < \theta < \frac{9\pi}{4} \\ (F(\theta) + f(\theta))\lambda_2 & \frac{9\pi}{4} \le \theta \end{cases} \tag{37}$$

The A-phase flux linkage is:

$$\varphi_{aa} = \int_{-\frac{3\pi}{4}}^{\frac{5\pi}{4}} B(\theta) w d\theta \tag{38}$$

For calculation convenience, the current is set to unit current, the A-phase is the flux, as shown in Table 2.

Table 2. A phase winding flux and self-induction.

Mover Position	$\boldsymbol{\varphi_{aa}}$	$\boldsymbol{L_{bb}}$
$\left[-\infty, -\frac{3\pi}{4}\right]$	$\int_{-\frac{3\pi}{4}}^{\frac{5\pi}{4}} F(\theta)\lambda_1 w \frac{\tau}{\pi} d\theta$	$L_{10} = 13.7130\ \lambda_1$
$\left[-\frac{3\pi}{4}, \frac{5\pi}{4}\right]$	$\int_{-\frac{3\pi}{4}}^{\theta} B(\theta) w \frac{\tau}{\pi} d\theta$	$\sum_{k=1}^{K=2} L_{20}\left(\frac{1}{k^2}\sin(\mathrm{k}\theta)\right)$
$\left[\frac{5\pi}{4}, \infty\right]$	$\int_{-\frac{3\pi}{4}}^{\frac{5\pi}{4}} F(\theta)\lambda_2 w \frac{\tau}{\pi} d\theta$	$L_{20} = 23.7130\ \lambda_2$

The connection of the magnetic flux in phase B is the same as in phase A, except that the phase difference is 90°.

$$\varphi_{bb} = \int_{-\frac{\pi}{4}}^{\frac{7\pi}{4}} B(\theta + \frac{\pi}{2}) w \frac{\tau}{\pi} d\theta \tag{39}$$

The mutual inductance is the magnetic flux intensity generated in the B-phase winding when the A-phase winding is energized. In this case, φ_{ab} is the magnetic flux in the B-phase winding when the A-phase winding is energized. φ_{ba} is the magnetic flux in the A-phase winding when the B-phase winding is energized. Due to the symmetrical structure of the two phases, they can be considered equal and are calculated as shown in Table 3.

$$\varphi_{ab} = \int_{-\frac{\pi}{4}}^{\frac{7\pi}{4}} B(\theta) w \frac{\tau}{\pi} d\theta \tag{40}$$

Table 3. AB phase winding flux and self-induction.

Mover Position	$\boldsymbol{\varphi_{ab}}$	$\boldsymbol{L_{ab}}$
$\left[-\infty, -\frac{\pi}{4}\right]$	$\int_{-\frac{\pi}{4}}^{\frac{7\pi}{4}} F(\theta)\lambda_1 w \frac{\tau}{\pi} d\theta$	$L_{30} = 3.7130\ \lambda_1$
$\left[-\frac{\pi}{4}, \frac{7\pi}{4}\right]$	$\int_{-\frac{\pi}{4}}^{\theta} \mathrm{B}(\theta) w \frac{\tau}{\pi} d\theta$	$\sum_{k=1}^{K=2} L_{40}\left(\frac{1}{k^2}\sin(\mathrm{k}\theta)\right)$
$\left[\frac{7\pi}{4}, \infty\right]$	$\int_{-\frac{1}{4}}^{\frac{7\pi}{4}} F(\theta)\lambda_2 w \frac{\tau}{\pi} d\theta$	$L_{40} = 6.7130\ \lambda_2$

5. Incremental Inductance Analysis of WS-PMLSM

The above analysis methods can calculate the linear and nonlinear characteristics of inductance, such as the nonlinear characteristics of the inductance for current and position, but are not suitable for incremental inductance. If incremental inductance is required (e.g., Equation (12)), a common method is the magnetic energy perturbation method, the key to this method is to find the magnetic field energy at the static operating point and calculate its absorption, then the incremental self-inductance of the i-phase winding of an n-phase wound motor can be expressed as:

$$L_{ii}^{in} = \frac{\partial^2 W_w}{\partial(\Delta i_i)^2} = \frac{\Delta W(i_i + \Delta i_i) + \Delta W(i_i - \Delta i_i)}{(\Delta i_i)^2} \tag{41}$$

where: L_{ii}^{in}—incremental inductance; W_w—total magnetic field energy; Δi_{ij}—current perturbation; ΔW—magnetic field storage energy perturbation. It is generally considered that $L_{ij}^{in} = L_{ji}^{in}$, then the incremental mutual inductance between phase i and phase j is:

$$M_{ij}^{in} = \frac{\Delta W\left(i_i+\Delta i_i, i_j+\Delta i_j\right)+\Delta W\left(i_i-\Delta i_i, i_j-\Delta i_j\right)}{4(\Delta i_i)\left(\Delta i_j\right)} - \frac{\Delta W\left(i_i+\Delta i_i, i_j-\Delta i_j\right)+\Delta W\left(i_i-\Delta i_i, i_j+\Delta i_j\right)}{4(\Delta i_i)\left(\Delta i_j\right)} \tag{42}$$

6. Experimental Analysis

6.1. Experimental Methods and Equipment

Figure 9 shows an inductance test system for a two-phase WS-PMLSM. The test bench contains the necessary instruments such as motor, LCR bridge, power supply, oscilloscope, and display. The parameters of the PMLSM are given in Table 1.

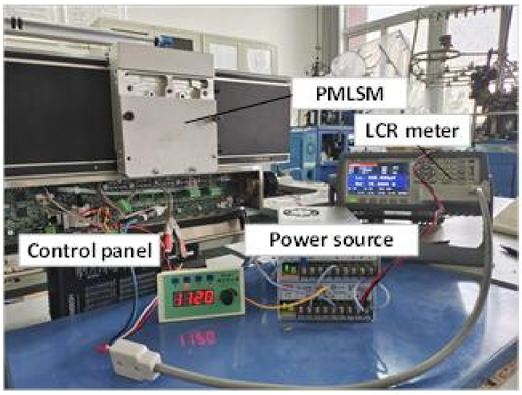

Figure 9. Experimental equipment.

The experimental method is as follows:

(1) The apparent inductance is measured using the conventional method of direct measurement of the self-inductance of the A and B phase windings using the LCR digital bridge.

(2) The mutual inductance of the A and B phase windings of the apparent inductor is accomplished by changing the circuit, i.e., when measuring the mutual inductance, the connection of the A and B phase windings needs to be changed, as shown in Figure 10, when the two windings are connected in the same direction, the equivalent inductance expression is $L_f = L_{Ah} + L_{Bh} + 2L_{ABh}$, when the two windings are connected in reverse, the equivalent inductance expression is:$L_r = L_{Ah} + L_{Bh} - 2L_{ABh}$, so, the mutual inductance of AB two-phase winding can be obtained by combining $L_{ABh} = \frac{L_f - L_r}{4}$.
Since the operation of LCR is relatively simple, we will not expand the description here, but we should pay attention to the selection of test frequency during the test. If the frequency is selected too high, the capacitive characteristics of the motor coil will be prominent and affect the inductance measurement results. In this paper, the test frequency is selected as 120 Hz.

(3) The incremental inductance is measured by the current differentiation method (di/dt). The segmented motor studied in this paper uses a surface-mounted permanent magnet structure, and the conductivity of the permanent magnet material is so small that the B

phase can be open-circuited when the A phase is in the test state, so the measurement conditions are met, and vice versa.

The current differentiation method is considered to be a better method to measure the phase inductance of the winding, the configuration and wiring are shown in Figure 11a.

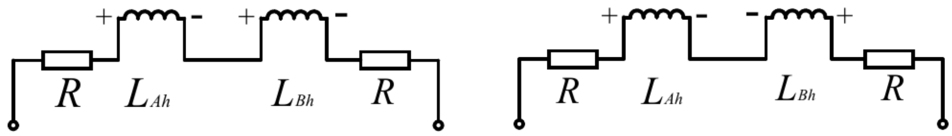

(**a**) Synthetic connection. (**b**) Reverse connection.

Figure 10. Mutual inductance measurement method.

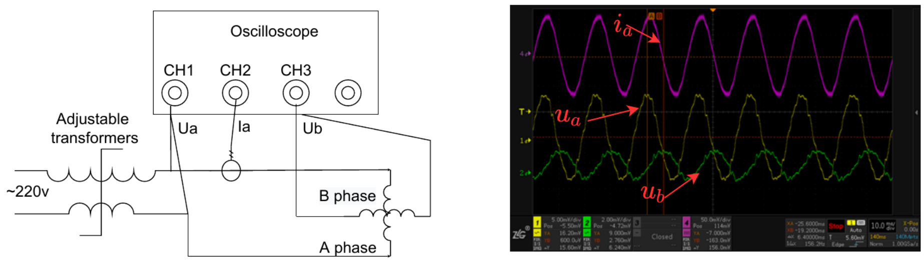

(**a**) Test system configuration and wiring diagram. (**b**) Experimental waveform.

Figure 11. Winding connection.

The adjustable transformer is powered by a sinusoidal AC of rated frequency and data acquisition is accomplished with an isolated three-channel oscilloscope ZDS4054. The inductance values of the rising as well as falling sinusoidal current waveforms were calculated by Equation (43) to Equation (44) and the average value is obtained as the RMS value. The calculation procedure uses the gradient equivalence principle to calculate the differential arithmetic.

$$L_{\mathrm{aa}} = \frac{U_{\mathrm{a}} - R_{\mathrm{a}} i_{\mathrm{a}}}{\mathrm{d}i_{\mathrm{a}}/\mathrm{d}t} \approx \frac{U_{\mathrm{a}} - R_{\mathrm{a}} i_{\mathrm{a}}}{\Delta i_{\mathrm{a}}/\Delta t} \tag{43}$$

$$M_{\mathrm{ab}} = -\frac{\psi_{\mathrm{b}}}{\partial i_{\mathrm{a}}} = \frac{-U_{\mathrm{b}}}{\mathrm{d}i_{\mathrm{a}}/\mathrm{d}t} \approx \frac{-U_{\mathrm{b}}}{\Delta i_{\mathrm{a}}/\Delta t} \tag{44}$$

6.2. Experimental Results

To complete the inductance analysis method, we use the LCR bridge method and the current differentiation method to implement, where the LCR verifies the apparent and positional inductance and the current differentiation method verifies the incremental inductance.

The waveforms of the apparent inductance are shown in Figure 12. The second harmonic frequencies of self-inductance and mutual inductance are the same, but the amplitudes are different, where the amplitude of mutual inductance is one-third of that of self-inductance, which is determined by the characteristics of the two-phase motor, indicating the superiority of the two-phase motor.

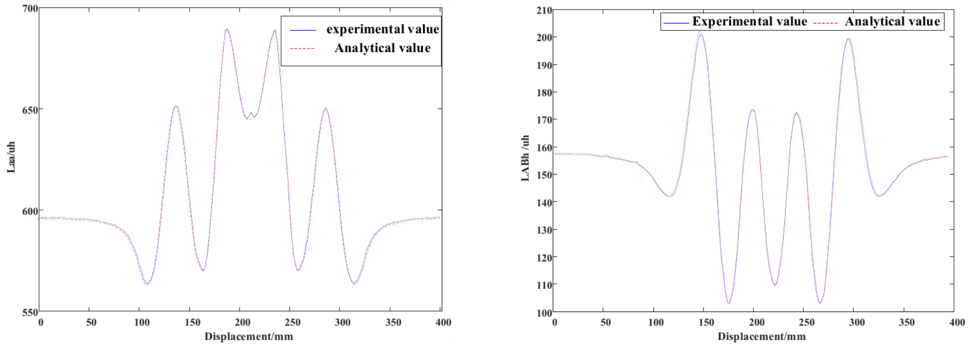

(**a**) A-phase self-inductance. (**b**) Mutual inductance of AB.

Figure 12. Inductance experimental waveform.

The waveform of position inductance is shown in Figure 13b, it is composed of the Sigmoid function and its derivatives, trigonometric functions, etc.

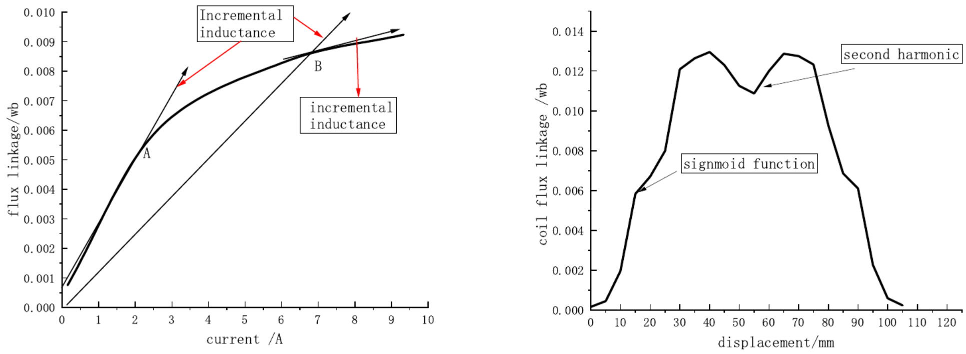

(**a**) Incremental inductance experiment. (**b**) position inductance experiment.

Figure 13. Two inductance waveforms.

The incremental inductance experiment is shown in Figure 13. At point A in Figure 13a, the incremental inductance is the same as the apparent inductance, but when the current reaches a saturation value during acceleration, as at point B in Figure 13a, the apparent inductance is not the same as the incremental inductance at this point. Therefore, a current differentiation term should be added to the control system to compensate for this change.

7. Conclusions

In this paper, a two-phase winding WS-PMLSM was discussed, and its model and electromagnetic parameters were analyzed. At the same time, based on the MMF function and the specific permeability function, the two-phase WS-PMSLM full-stroke inductance analytical model was derived, the main conclusions obtained are as follows:

(1) The second harmonic of the self-inductance of the two-phase winding designed in this paper is very small, and the higher harmonics are even less.
(2) In the fully coupled state, the amplitude ratio of the DC components of mutual inductance and self-inductance of the A and B phase windings is unchanged, and the mutual inductance is one-third of the self-inductance, and the mutual inductance under the *dq*-axis is basically zero, and the vector control with general feedforward can be used for occasions with low requirements.
(3) In the full travel range, the DC components of the self and mutual inductance of the A and B phase windings with the second harmonic amplitude decrease as the motor coupling length decreases, which is basically linear, unlike the motor with three-phase winding.

(4) Inductance is available in two cases viz: $\mathbf{L}_{\mathrm{dq}}^{\mathrm{diff}}$ and $\partial\mathbf{L_{dq}}/\partial x$, $\mathbf{L}_{\mathrm{dq}}^{\mathrm{diff}}$ consisting of apparent inductance and incremental inductance, in the linear region, they are equal, but in the saturation region, they are not equal, so it is necessary to take a reasonable way in high acceleration and deceleration control, $\partial\mathbf{L_{dq}}/\partial x$ is basically a constant.

(5) The role of inductance in different controls is different, so pay attention to the trade-offs.

In conventional vector control, after dq conversion, the inductors are completely decoupled and the feedforward caused by the motor parameters is exact, as shown in Figure 14a, this is the conventional dq model with the equation shown in Equation (45). From both the equation and the diagram it can be seen that the inductance is completely decoupled from the position, the current control is also decoupled and the accuracy of the system depends on the identification of the motor parameters, despite this, the first harmonic of the inductance is also required to be constant.

$$\begin{cases} u_d = Ri_d + L_d \frac{\mathrm{d}}{\mathrm{d}t} i_d - \omega_\mathrm{e} L_q i_q \\ u_q = Ri_q + L_q \frac{\mathrm{d}}{\mathrm{d}t} i_q + \omega_\mathrm{e} (L_d i_d + \psi_\mathrm{f}) \end{cases} \tag{45}$$

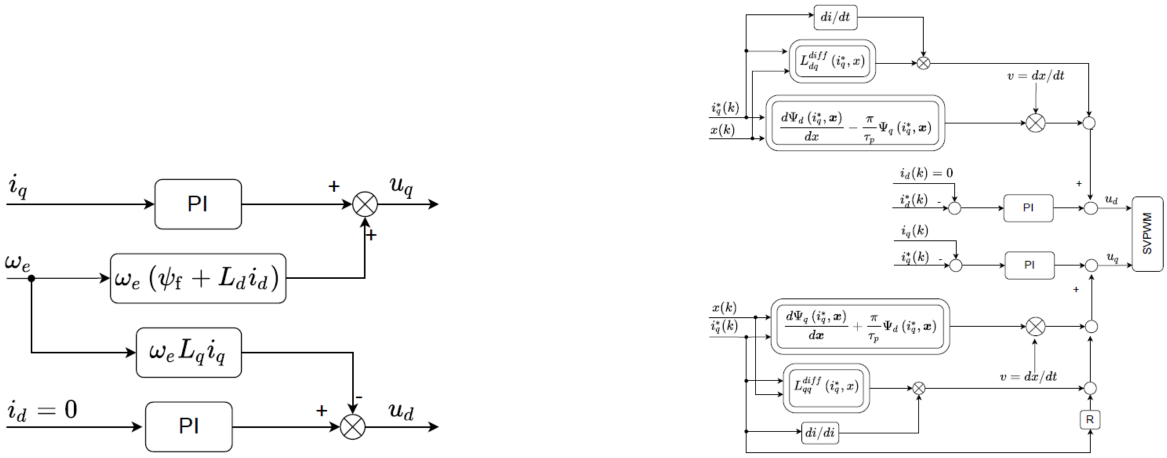

(**a**) Control method without considering inductance change. (**b**) Control method with considering inductance change.

Figure 14. Consider two control methods for inductors.

In the WS-PMLSM, the inductance is no longer constant, from the frequency domain point of view, it contains multiple harmonics, from the inductive component, it contains three kinds of inductance as analyzed above, its mathematical model is given as Equation (15), and the unfolding control block diagram is given in Figure 14b. Therefore, for the inductance problem of WS-PMLSM, the three-dimensional inductance look-up table method is common, and the nonlinear curve fitting method and artificial intelligence are also used, which will not be expanded on here.

Author Contributions: T.Z. proposed the main ideas, wrote the paper, designed the whole framework. X.M. provided guidance for the work, reviewed the paper, and acquired funding. All authors have read and agreed to the published version of the manuscript.

Funding: This work was supported in part by the National Natural Science Foundation of China under the grant 51735010.

Institutional Review Board Statement: Not applicable.

Informed Consent Statement: Not applicable.

Data Availability Statement: The dataset can be accessed upon request to the corresponding author.

Conflicts of Interest: The authors declare no conflict of interest.

References

1. Rassudov, L.; Tolstikh, O.; Tiapkin, M.; Paskalov, N.; Korunets, A.; Osipov, D. Digital Twin Implementation for Accelerating the Development of Flexible Transportation System Control Software. In Proceedings of the 2021 IEEE 62nd International Scientific Conference on Power and Electrical Engineering of Riga Technical University (RTUCON), Riga, Latvia, 15 November 2021; pp. 1–4. [CrossRef]
2. Zhang, T.; Du, X.; Mei, X. Modelling and Analysis of Two-Phase Winding Segmented Permanent Magnet Linear Synchronous Motor. In Proceedings of the 2021 13th International Symposium on Linear Drives for Industry Applications (LDIA), Wuhan, China, 1–3 July 2021; pp. 1–6. [CrossRef]
3. Benavides, R.; Mutschler, P. Detent force compensation in segmented long stator permanent magnet linear drives using Finite Element Models. In Proceedings of the 2007 European Conference on Power Electronics and Applications, Aalborg, Denmark, 2–5 September 2007; pp. 1–10.
4. Mutschler, P. Comparison of topologies for linear drives in industrial material handling and processing applications. In Proceedings of the 2007 7th Internatonal Conference on Power Electronics, Aalborg, Denmark, 2–5 September 2007; pp. 1027–1032.
5. Rovers, J.; Jansen, J.; Lomonova, E. Novel force ripple eduction method for a moving-magnet linear synchronous motor with a segmented stator. In Proceedings of the 2008 International Conference on Electrical Machines and Systems, Wuhan, China, 17–20 October 2008; pp. 2942–2947.
6. Benavides Oswald, R. Investigation of Control Methods for Segmented Long Stator Linear Drives. Ph.D. Thesis, Technische Universität, Darmstadt, Germany, 2008.
7. Hall, D.; Kapinski, J.; Krefta, M.; Christianson, O. Transient electromechanical modeling for short secondary linear induction machines. *IEEE Trans. Energy Convers.* **2008**, *23*, 789–795. [CrossRef]
8. Tan, Q.; Wang, M.; Li, L.; Li, J. Pulsating magnetic field of permanent magnet linear synchronous motor and its influence on detent force. *IEEE Trans. Energy Convers.* **2020**, *36*, 703–712. [CrossRef]
9. Lu, Q.; Wu, B.; Yao, Y.; Shen, Y.; Jiang, Q. Analytical model of permanent magnet linear synchronous machines considering end effect and slotting effect. *IEEE Trans. Energy Convers.* **2019**, *35*, 139–148. [CrossRef]
10. Cui, L.; Zhang, H.; Jiang, D. Research on High Efficiency V/f Control of Segment Winding Permanent Magnet Linear Synchronous Motor. *IEEE Access* **2019**, *7*, 138904–138914. [CrossRef]
11. Wang, M.; Kang, K.; Zhang, C.; Li, L. A Driver and Control Method for Primary Stator Discontinuous Segmented-PMLSM. *Symmetry* **2021**, *13*, 2216. [CrossRef]
12. Junjie, H.; Donghua, P.; Zhijian, Z. Comparison of the two current predictive-control methods for a segment-winding permanent-magnet linear synchronous motor. *IEEE Trans. Plasma Sci.* **2013**, *41*, 1167–1173.
13. Queval, L.; Ohsaki, H. Nonlinear abc-model for electrical machines using N-D lookup tables. *IEEE Trans. Energy Convers.* **2014**, *30*, 316–322. [CrossRef]
14. Perreault, B.M. Optimizing operation of segmented stator linear synchronous motors. *Proc. IEEE* **2009**, *97*, 1777–1785. [CrossRef]
15. Molano, J.C.C.; Capelli, L.; Rubini, R.; Borghi, D.; Cocconcelli, M. A bearing fault model for Independent Cart Conveyor System and its validation. *Appl. Acoust.* **2020**, *159*, 107069. [CrossRef]
16. Zhu, Z.; Howe, D.; Mitchell, J. Magnetic field analysis and inductances of brushless DC machines with surface-mounted magnets and non-overlapping stator windings. *IEEE Trans. Magn.* **1995**, *31*, 2115–2118. [CrossRef]
17. Wang, J.; Jewell, G.W.; Howe, D. A general framework for the analysis and design of tubular linear permanent magnet machines. *IEEE Trans. Magn.* **1999**, *35*, 1986–2000. [CrossRef]
18. Chiba, A.; Nakamura, F.; Fukao, T.; Rahman, M.A. Inductances of cageless reluctance-synchronous machines having nonsinusoidal space distributions. *IEEE Trans. Ind. Appl.* **1991**, *27*, 44–51. [CrossRef]
19. Dutta, R.; Rahman, M.; Chong, L. Winding inductances of an interior permanent magnet (IPM) machine with fractional slot concentrated winding. *IEEE Trans. Magn.* **2012**, *48*, 4842–4849. [CrossRef]
20. Liu, C.; Wang, H.; Zhang, Z.; Shen, X. Research on thrust characteristics in permanent magnet linear synchronous motor based on analysis of nonlinear inductance. *Proc. CSEE* **2011**, *30*, 69–76.
21. Jikun, Y.; Liyi, L.; Jiangpeng, Z. Analytical calculation of air-gap relative permeance in slotted permanent magnet synchronous motor. *Trans. China Electrotech. Soc.* **2016**, *31*, 45–52.
22. Liyi, L.; Mingna, M.; Jiaxi, L.; Chan, C. Inductance analysis in pass-through section for multi-segmented permanent magnet linear motors based on magnetic energy perturbation. *Trans. China Electrotech. Soc.* **2013**, *28*, 46–55.
23. Zhang, H.; Chen, G.; Zhang, K. Analytical calculation of Permanent Magnet Flux Linkage and Winding Inductance of Mover Permanent Magnet Double Salient Reluctance Linear Machines. In Proceedings of the 2021 IEEE 4th Student Conference on Electric Machines and Systems (SCEMS), Hangzhou, China, 1–3 December 2021; pp. 1–7.
24. Shujun, M.; Jianyun, C.; Xudong, S.; Shanming, W. Analysis and Restrain of Mutual Inductance Asymmetry in the Sectionally Powered AC Linear Motor. *Trans. China Electro Tech. Soc.* **2015**, *30*, 81–88.
25. Ma, M.; Li, L.; Zhang, J.; Yu, J.; Zhang, H. Investigation of cross-coupling inductances for long-stator PM linear motor arranged in multiple segments. *IEEE Trans. Magn.* **2015**, *51*, 1–4.